METRO: Magnetic Road Markings for All-weather, Smart Roads

Jike Wang†, Shanmu Wang†, Yasha Iravantchi◇, Mingke Wang◇
Alanson Sample◇, Kang G. Shin◇, Xinbing Wang†, Chenghu Zhou‡, Dongyao Chen†*
† Shanghai Jiao Tong University, ‡ Chinese Academy of Sciences
{jikewang,wangshanmu,xwang8,chendy}@sjtu.edu.cn,zhouch@lreis.ac.cn
◇ University of Michigan, Ann Arbor
{yiravan,mingkew,apsample,kgshin}@umich.edu

ABSTRACT

Road surface markings, like symbols and line markings, are vital traffic infrastructures for driving safety and efficiency. However, real-world conditions can impair the utility of existing road markings. For example, adverse weather conditions such as snow and rain can quickly obliterate visibility.

We propose a novel MagnETic ROad marking system (METRO) for robust recognition of road markings at low cost and high deployability. METRO pairs (a) easily deployable passive magnetic road markings with (b) an automotive-grade magnetic sensing framework that detects and interprets these markings. The design of METRO addresses several real-world challenges, such as mitigating the impact of magnetic disturbances, lowering deployment costs, and enhancing the durability of magnetic tags. On-road field tests of METRO demonstrate an overall accuracy of over 96% in interpreting various road markings in adverse conditions with less cost (only $0.17 per meter) than traditional road markings ($0.21-7.70 per meter). Our field evaluation of METRO over one month demonstrates the practicality and robustness of METRO in real-world settings. Specifically, we observed no performance degradation in the METRO sensor array and no damage or demagnetization to METRO's magnetic tags.

CCS CONCEPTS

• **Hardware → Sensor devices and platforms**.

KEYWORDS

Magnetic sensing; all-weather road markings; magnetometer

ACM Reference Format:
Jike Wang†, Shanmu Wang†, Yasha Iravantchi◇, Mingke Wang◇, Alanson Sample◇, Kang G. Shin◇, Xinbing Wang†, Chenghu Zhou‡, Dongyao Chen†*. 2023. METRO: Magnetic Road Markings for All-weather, Smart Roads. In *ACM Conference on Embedded Networked Sensor Systems (SenSys '23), November 12–17, 2023, Istanbul, Turkiye.* ACM, New York, NY, USA, 14 pages. https://doi.org/10.1145/3625687.3625809

*Dongyao Chen is the corresponding author.

SenSys '23, November 12–17, 2023, Istanbul, Turkiye

ACM ISBN 979-8-4007-0414-7/23/11…$15.00
https://doi.org/10.1145/3625687.3625809

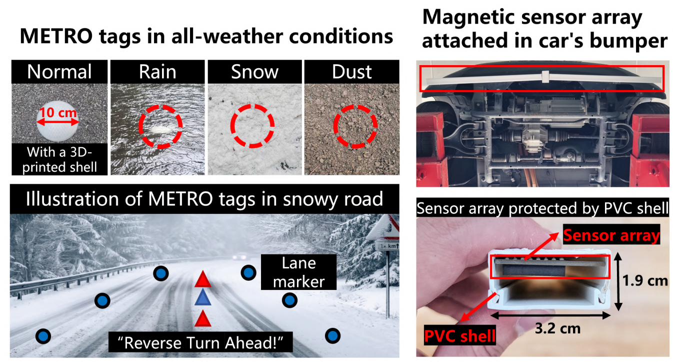

Figure 1: METRO comprised of highly deployable, all-weather magnetic dots and a novel sensor array.

1 INTRODUCTION

Road surface markings have been an indispensable part of traffic infrastructure to improve driving safety and efficiency for over 100 years [6]. Lane markers, symbols, and texts guide and inform drivers, pedestrians, and cyclists. For example, lane markers divide the road for traffic flow. Symbols (e.g., bicycle lanes and arrows) and text (e.g., road names and alerts) give drivers concise navigational and safety guidance. Nowadays, identifying road markings accurately is critical for the success of advanced driving technologies. For example, autonomous vehicles and advanced driver-assistance systems (ADAS) process imaging data to properly steer and perform lane-departure maneuvers.

Historically, pavement markings have focused on improving the visibility of paintings on the road. Yet, the visibility can easily degrade in real-world conditions. In particular, snow, rain, and fog impair the visibility and/or retro-reflectivity of the markings [55]. Painted road markings can wear out due to the sun's glare and temperature changes [33]. Despite the recent advances [38, 81] in computer vision, prior work [59] using high-quality vehicular cameras has shown adverse weather conditions severely undermine the performance of ADAS and self-driving cars. Hence, the limited visibility is a critical weakness for road markings [5].

Traffic engineering researchers have proposed several ways to mitigate the impact of poor visibility. As we will elaborate in Sec. 2, mechanical road markings (cat's eyes [54] and raised pavement markers [46]) provide enhanced retro-reflectivity and tactile feedback to alert drivers. However, these markers convey limited information and may still be occluded by accumulated snow [9]. Raised markers that can withstand snow removal by snow plows remain too costly for large-scale deployment [57]. Camera-free methods, such as RFID [44, 58] and mmWave [56, 66], have been proposed to enhance roadside signs. However, as we elaborated in Sec. 2.2 and Sec. 7.3, these methods suffer from several key issues, such as signal distortion due to the multi-path effect in *high-speed* scenarios and high deployment costs. Passive magnetic pavements have been deployed on the road to facilitate vehicle posture estimation and achieve road tracking [16, 34, 36, 47, 49]. However, such systems require vehicles to follow the magnetic path strictly and can not encode rich road information.

We present METRO, a novel all-weather road marking infrastructure. By leveraging magnetic sensing, this framework enables METRO unique resilience against adverse conditions (e.g., water, snow, and dust), thus enabling accurate, robust, and cost-efficient perception of road markings, as shown in Fig. 1. At its core, METRO consists of two key modules:

- **Passive magnetic tag:** METRO employs a novel design of magnetic tags that can be built and deployed on the *real road* at a *low cost*;
- **Magnetic sensing module:** To accurately decode magnets, we propose a new design for magnetometer array attached to the front of the car's undercarriage. We also design a tailored sensing algorithm robust to various real-world driving conditions.

The design of METRO tackles several challenging questions:

How to denote various road markings with passive magnets effectively? It is extremely challenging to denote road markings with passive magnets. Information can be encoded using magnets by switching N/S polarities. However, only employing permutations of polarities results in a limited encoding capacity. For example, only eight different messages can be encoded with three magnets. We propose a cost-effective encoding scheme to vastly increase the amount of information that can be encoded using a restricted number of magnets. As elaborated in Sec. 4, METRO employs a series of magnets and leverages the polarity orientation (i.e., the 3D orientation of the N/S pole) of each magnet to encode the line markings (e.g., dashed line and solid line) at an extremely low cost of only $0.17 per meter. To encode information markings, we utilize both the polarity orientation and the distance between magnets. By varying the polarity orientation and the inter-magnet distance, METRO can encode rich information. For example, a tag prototype consisting of three magnets spaced across 4 m can encode more than 248 unique messages at a cost of only $3. We also propose an efficient manufacturing and deployment process for METRO. A METRO tag can be easily deployed in real-world roads to digitize legacy road markings (Sec. 8.2).

How to achieve robust magnetic sensing? The vicinity of a magnet can be detected with MEMS magnetometers [53] — a compact and energy-efficient magnetic field sensor. However, the magnetic field strength degrades rapidly with the distance between the magnet and the sensor [70]. The sensing algorithm should decode METRO tag, i.e., detect the polarity and the inter-magnet distance, with high accuracy. This is challenging when the sensor is mounted on a car moving with varying heading and high velocity (e.g., > 50 mph). METRO reader should also overcome real-world disturbances (e.g., adverse weather, rough roads, by-passing cars, metal covers of maintenance holes) that may degrade the sensing performance. To meet these challenges, we propose an automotive-grade magnetic sensing framework that constitutes novel hardware and software designs. For the hardware design, we propose a low-cost (< $85) and easy-to-use magnetometer sensor array platform. For the software design, we present a highly accurate and low-latency (< 25 ms) sensing algorithm for decoding those tags.

We conducted extensive field tests in various real-world settings. Specifically, we have evaluated METRO's performance in different temperatures, varying vehicle velocity, heading, and ground clearance settings. We have also evaluated METRO's performance in different road conditions, including rough pavements, curvy roads, and emulated snow-covered scenarios. We have conducted field tests of METRO on commodity vehicles and public roads for a month in real-world conditions. These empirical results demonstrate METRO's practicality and robustness in real-world/harsh road environments. METRO's performance demonstrates unique advances as the next-generation road markings. Therefore, it has the potential to open the door to smart roads and the future transportation ecosystem. We have also open-sourced all design and analytical techniques of METRO [20] for the community to reproduce the results.

In summary, this paper makes the following contributions:

- Development of METRO, the first practical and cost-effective magnetic road marking design for all-weather and smart roads;
- Design of a novel magnetic encoding scheme to efficiently encode road markings with passive magnets;
- Design of METRO's sensing module;
- Extensive field tests to verify the accuracy, practicability, and deployability of METRO in the real world.

2 BACKGROUND AND MOTIVATION

2.1 Primer of Road Markings

Road markings are indispensable for providing guidance and safety information, including longitudinal and transverse markings [30]. Longitudinal pavement markings are essential for guiding the forwarding movement of vehicles, such as lane lines, center lines, edge lines, etc. Transverse markings contain a large amount of complex road information, such as pavement words, symbols, and arrow markings, for guiding, warning, or regulating traffic. In the daytime, the visibility of these road markings is based on the color contrast between the marking and the road. At night time, when the amount of light available to the drivers is limited, the retro-reflectivity of road markings provides luminous contrast between markings and the road surface.

2.1.1 Visibility of road markings. Prior work strived to enhance the visibility of road markings for road safety [65, 82]. A straightforward approach is to enhance the marker's retro-reflectivity. For example, epoxy paints and thermoplastic markings offer higher retro-reflectivity than regular paints with higher manufacturing and labor costs [40]. To further enhance the retro-reflectivity, convex markers have been proposed to achieve a larger angle of reflection. For example, cat's eyes [54] help reflect the vehicle's headlight; convex dots (e.g., Botts' dots [1]) have a reflective surface to enhance their visibility.

However, all vision-based markers are susceptible to the distortion of visibility. Specifically, the visibility can be obliterated by rain, snow, debris, and water. Although the convexity of mechanical tags can also enable tactile feedback (i.e., vibration), these tags convey only limited information, like lane departure warning (LDW), to the driver. Note that vibration alerts can also be obliterated by the accumulated snow and/or ice. The above limitations undermine the performance of legacy road markings in the real world. Therefore, vision-free sensing of road markings would be essential for all-weather/condition traffic safety and efficiency.

2.2 Why Magnetic Sensing?

2.2.1 State-of-the-art camera-free approaches. To overcome the limited visibility of road infrastructure, camera-free techniques like RFID, NFC, and mmWave have been proposed.

Researchers explored the use of active and passive RFID tags [58, 60] for detecting road signs. However, for the following limitations, RFID technology is ill-suited for recognizing the information embedded in *road surfaces for high-speed vehicles.* **(A) High-cost RFID readers and tags.** RFID readers are usually expensive, costing over $1,000 [41], which can severely limit their large-scale deployment. In contrast, the METRO sensor array is much cheaper (< $85 as elaborated in Sec. 8.1). RFID tags are also sensitive to minor variations in the environment or tag geometry, i.e., changes in an RFID tag's orientation or flexing [74]. Rugged RFID tags necessary for harsh environments are expensive, costing > $8 per tag [21]. Magnets are more durable and much cheaper, only $1 apiece as shown in Sec. 8.1. **(B) Sensing accuracy in high-speed, rough on-road settings.** The interference caused by multiple lane- and information-markers in the vicinity of an RFID reader could cause false detections. Building retro-directive RFID tags is challenging due to the large antenna size required in the UHF band [56]. Moreover, existing localization schemes, including measuring the received signal phase [32, 63, 79] and the received signal strength (RSS) [43, 64, 73] are not robust in high-speed scenarios. Specifically, phase-based methods can suffer severely from multi-meter errors in non-line-of-sight (NLOS) environments due to the signal reflection by obstacles [74, 75]. RSS is highly vulnerable to the multi-path effect caused by environmental interference [74]. Our experiments in Sec. 7.3 also show watery disturbance to distort RSS significantly. In contrast, magnetic sensing is resilient against adverse conditions. METRO also demonstrates high sensing accuracy in high-speed scenarios.

NFC systems are ill-fitted for real-world on-road applications. NFC techniques leverage principles of inductive magnetic coupling [62]. The communication range of these systems is less than 10 cm [69]. [80] enables the NFC tags to read at a distance of up to 3 m. However, the moving speed is constrained to only 1 m/s.

Recently, researchers proposed high-frequency millimeter-wave techniques [56, 66, 78] for interpreting roadside traffic signs. However, these methods were inapplicable to road surfaces. Specifically, on-road reflective objects, including water and bypassing cars would create severe multi-path effects, thus attenuating the received signal.

2.2.2 Background of magnetic sensing. Magnetic sensing is an emerging technique that senses passive magnets with MEMS magnetometer(s) [37, 76]. Compared to existing methods, magnetic

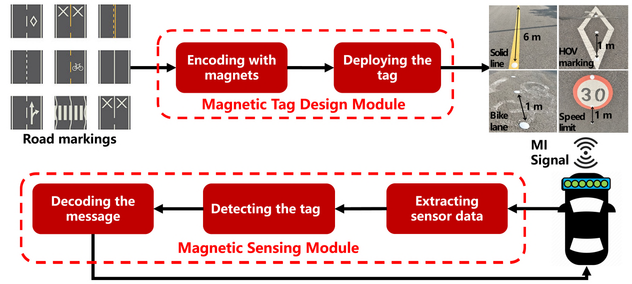

Figure 2: System overview of METRO.

sensing has the following advantages making it ideal for digitizing road markings.

- **Reliability.** Magnetic field is resilient to the NLOS problem. It is not affected by weather conditions.
- **Durability.** Passive magnets are durable. This is a crucial feature for road surface deployment.
- **Cost efficiency.** Compared to RF approaches, MEMS magnetometers and passive magnets incur a minimal cost for purchasing and installation.

However, there are two major difficulties in encoding and detecting road markings via magnetic sensing. First, it is difficult to encode diverse road information with passive magnets cost-effectively. Prior works on magnetic guidance have employed magnetic stripes guiding vehicles [16, 34, 36, 47]. However, these approaches are limited to encoding rich road information. Second, how to reliably detect magnetic markings with COTS magnetometers? We will address these two challenges in the remainder of the paper.

3 OVERVIEW OF METRO

Fig. 2 shows a system overview of METRO which consists of two key modules: magnetic tags and a magnetic sensing unit. One first encodes road markings with passive magnets (Sec. 4). Then, it presents a low-cost deployment scheme for these magnetic tags (Sec. 6.3). For robust detection of on-road magnetic tags, METRO implements an automotive-grade magnetic sensing module, including a low-cost and easy-to-use hardware design (Sec. 5.1) and a novel derivative-based peak detection algorithm (Sec. 5.2) with built-in noise cancellation scheme (Sec. 5.3). Based on these two modules, METRO can achieve all-weather perception of road markings.

4 DESIGN OF METRO TAG

4.1 Encoding Longitudinal Markings

We focus on two types of longitudinal markings, i.e., dashed and solid lines. These line settings are seminal road markings. A specific magnetic lane tag for longitudinal marking is modeled as a tuple $\{P, \phi\}$, where P is the polarity, i.e., "N" or "S", and ϕ is the polarity orientation. We determine the orientation by analyzing the magnetic field distribution of passive magnets. Specifically, the strongest magnetic field of a passive magnet is at its N/S pole due to the highest magnetic flux density [70]. A magnet would more likely be detected by the magnetometer when its pole points at the sensor. Hence, we set the magnet with the N/S polarity for the upside, i.e., $\phi = 90°$, as shown in Fig. 3(a), for these more safety-critical markings. To this end, a series of magnets of {"N", 90°} configuration can

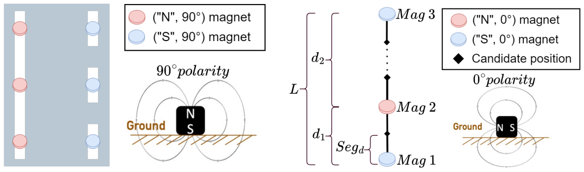

(a) Longitudinal markings (b) Transverse markings

Figure 3: Magnetic tags encoded by METRO. (a) Longitudinal markings: $\{N, 90^{\circ}\}$ and $\{S, 90^{\circ}\}$ indicate solid and dashed lines, respectively. (b) An exemplary transverse marking denoted as $\{SNS,\ 0^{\circ},\ 3,\ L,\ Seg_d,\ d_2/d_1\}$.

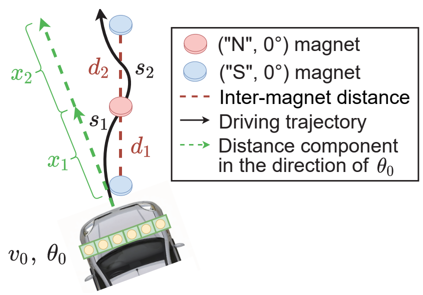

Figure 4: The vehicle motion when detecting a tag.

be the solid line. Similarly, we use a series of {"S", 90°} magnets for the dashed line. This design allows the driver or automotive system to have a timely reaction. For example, the driver should be alerted upon METRO reader's detection of a {"N", 90°} magnet.

4.2 Encoding Transverse Markings

Compared to longitudinal markings, transverse markings contain large amounts of road information. The key problem is how to reliably encode rich information with a minimal number of magnets. To tackle this problem, METRO introduces distance ratio, a novel encoding factor based on distance information. Specifically, a transverse marking is regarded as a tuple $\{P, \phi, M, L, Seg_d, r\}$, where P and ϕ are the same in lane tags, M is the number of magnets, L is the tag length, Seg_d is segmentation distance, r is the distance ratio.

Polarity design. The polarity orientation of transverse markings is forward (i.e., $\phi = 0^{\circ}$ relatives to the ground, as shown in Fig. 3(b)) aligned with the traffic direction. Thus, upon detection of the first 0° magnet, the detection effort will continue until the last magnet is found.

Distance ratio design. The encoding capacity would be limited with the use of polarity only. A large number of magnets would significantly increase the deployment cost. To mitigate this problem, METRO encodes information by tuning both polarity and inter-magnet distance. To retrieve accurate distance information, we propose two steps: (1) analyze the vehicle motion in real time with CAN bus data; (2) employ the distance ratio, i.e., the ratio of different segments.

Due to the arbitrary driving trajectory when detecting magnets, driving distance calculated only with speed data from the vehicle's CAN bus may not be equal to the inter-magnet distance, e.g., $s_2 \neq d_2$ in Fig. 4. To tackle this problem, we leverage the heading angle from the vehicle's CAN bus. Specifically, if we know the initial heading angle θ_0 when the first magnet is detected, we can calculate the distance components in the direction of θ_0, e.g., x_1 and x_2 in Fig. 4, respectively. The ratio of the distance components is approximately equal to the ratio of the inter-magnet distance (i.e., $x_2/x_1 \approx d_2/d_1$ in Fig. 4) for a specific information tag. Thus, with the speed and heading data from the CAN bus, we can derive the distance component accurately. For a tag consisting of M magnets, the number of segmentation is $M-1$. For the i^{th} segmentation, we can calculate the distance component x_i in the direction of θ_0 by leveraging five key pieces of information: polarity index p_i of the i^{th} magnet, p_{i+1} of the next magnet in the time-series data, sample rate f, speed v, and heading angle θ. Its calculation formula is:

$$x_i = \sum_{j=p_i}^{p_{i+1}} v_j \cos|\ \theta_j - \theta_0\ | \cdot \frac{1}{f} \tag{1}$$

The distance ratio of total $M-1$ segmentation can then be calculated by $x_1 : x_2 \cdots x_{M-1}$, which is approximately equal to $d_1 : d_2 \cdots d_{M-1}$. Let us elaborate on the inter-magnet distance setting scheme for an information tag with given L and M. The first and the last magnets are fixed/stationary as reference nodes. We only move the remaining $M-2$ magnets to derive different distance ratios. Specifically, we divide the length L into several candidate segments by utilizing the segmentation distance Seg_d as shown in Fig. 3(b). Then, $M-2$ magnets can be deployed in total $L/Seg_d - 1$ positions. For example, with a length of 4 m and a segmentation distance of 1 m, there are three candidate ratios: $r = 3/1, 2/2, 1/3$.

Encoding capacity analysis. For given M, L, Seg_d, the total number of polarity configurations are 2^M and the number of the possible positions is $L/Seg_d - 1$ for $M-2$ magnets. Thus, without magnetic field coupling, the ideal encoding capacity can be calculated by:

$$C = 2^M \cdot \binom{L/Seg_d - 1}{M-2} \tag{2}$$

where $\binom{L/Seg_d - 1}{M-2}$ represents the combination types for $M-2$ magnets from $L/Seg_d - 1$ candidate positions.

We analyze the impact of L, M, and Seg_d on encoding capacity using Eq. (2). Obviously, the tag length L contributes linearly to the encoding capacity. The effects of M and Seg_d are plotted in Fig. 5. As shown in Fig. 5(a), with $L = 4$ and $Seg_d = 0.5\ m$, we can achieve an encoding capacity of 2688 with only 7 magnets. When $M > 7$, the encoding capacity decreases because the combination of $M-2$ magnet positions from a total of $L/Seg_d - 1 = 7$ candidate positions reduces with more magnets. As shown in Fig. 5(b), a small segmentation distance yields high encoding capacity. With $M = 3$, $L = 4\ m$, METRO supports encoding 312 types of road information when $Seg_d = 0.1\ m$. As we will elaborate in Sec. 7, METRO's sensing pipeline is able to differentiate the ratio at fine granularity, indicating the practicability of encoding rich information with METRO.

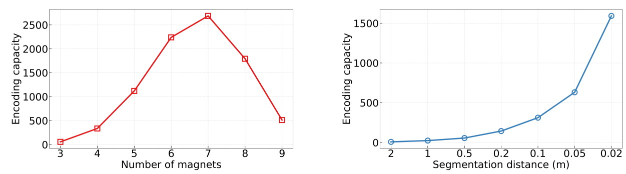

(a) Varying M, $L = 4\ m$, $Seg_d = 0.5\ m$ (b) Varying Seg_d, $M = 3$, $L = 4\ m$

Figure 5: The encoding capacity with different factors.

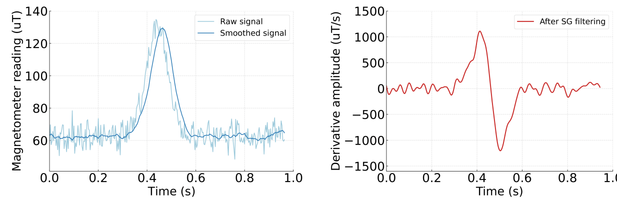

(a) Raw peak signal (b) First derivative signal

Figure 6: (a) shows the smoothed peak signal; (b) shows the derivative of the smoothed peak.

5 SENSING PIPELINE OF METRO

METRO needs to tackle several unique challenges to facilitate the harsh on-road scenarios. In particular, high speed (e.g., > 50 mph), adverse weather, and rough pavements. We propose an *automotive-grade* magnetic sensing pipeline for interpreting on-road magnetic tags, consisting of a novel hardware design and a robust sensing algorithm.

5.1 Hardware Design

We focus on three key design goals, high sensing accuracy, robust sensing reliability, and low manufacturing cost. To detect on-road magnets, we propose a one-layer bar layout of the sensor array. Placing all magnetometers in one layer facilitates their installation on vehicles. Next, we need to determine the inter-magnetometer distance. To balance the trade-off between detection performance and cost, based on our empirical study, the inter-magnetometer distance is determined to be 16 *cm*. The average vehicle width is around 5.8 ft (1.77 *m*) [12]. In the design of METRO, a total of 12 magnetometers (to fit a 1.77 *m* sensor array) are used for detecting magnetic tags. As we will show in Sec. 6, this distance is also suitable for the magnetic field strength of METRO tag. We can, of course, change the number of sensors to fit different car types (Sec. 6.1).

5.2 Sensing Algorithm

Based on the hardware design, we propose a high-accuracy and low-latency (< 25 ms) sensing pipeline for decoding rich lane-specific information from passive magnets. It includes two key modules: magnetic tag detection and identification.

5.2.1 Magnet detection. As described in Sec. 4, we encode information by leveraging the N/S polarities. A straightforward method is to detect the peak from the time-series magnetic field data. However, it is not feasible in practice to set a fixed threshold for detecting the peak because the magnetic field strength varies with road conditions and driving behaviors.

To handle this difficulty, we develop and implement a novel peak detection algorithm based on the first and second derivatives of the raw data. We notice that the first derivative of a peak has a downward zero-crossing point at the peak maximum, while the first derivative of a valley has an upward zero-crossing point. Compared to the direct use of raw data, the derivative eliminates the offset resulting from the varying environmental magnetic fields and different sensor configurations. This is the core that enables METRO to operate in *high-speed scenarios*. Our approach consists of three key steps: preprocessing, derivation, and peak/valley detection.

Step 1, Preprocessing. We first apply a Gaussian kernel smoother to denoise the real-time magnetometer data, as shown in Fig. 6(a). We propose a low-latency scheme for adaptively setting the speed-aware denoise window size. Specifically, we set the window size to 15 and 5 for slow (< 20 mph) and fast (> 40 mph) scenarios, respectively. We set the window size to 9 points for other speeds. Based on our empirical results, at more than 350 Hz sample rate, the maximal delay caused by this step is less than 20 ms.
Step 2, Derivation. After the data preprocessing, we calculate the first derivative of the smoothed data by using a Savitzky-Golay (SG) filter [61]. Specifically, we initially apply the SG filter to smooth the differential data of the peak signal. The window size is set to 5 points, and the polynomial order to fit the samples is 2 through our empirical study. Then, we can calculate the first derivative data by dividing the filtered differential data by the sample interval. This way, most undesired zero-crossing points and high-frequency noises can be effectively eliminated, as shown in Fig. 6(b), with a maximal time delay of less than 5 ms.
Step 3, Peak/Valley detection. The peak/valley can be detected reliably by searching for the downward/upward zero-crossing points in the first derivative data. To eliminate the false zero-crossing points incurred by random noises, we introduce the slope data of the derivative data and implement a threshold-based detection algorithm. The slope caused by the noise is smaller than that by the magnet, so we first calculate the slope for each zero-crossing point pair. We then initialize the slope threshold that reflects the impact of the surrounding environment. Finally, the slope exceeding this threshold implies a candidate magnet. To further eliminate false alerts, we introduce an amplitude threshold for each candidate zero-crossing point. Specifically, we compare the amplitude difference between the raw candidate data point and a preset value based on the magnet with the threshold.

5.2.2 Tag identification. The peak detection algorithm can find peaks robustly. To distinguish two types of tags (i.e., lane tags and information tags), we use two corresponding axes data based on the specific orientation of magnets. Specifically, the x-axis peak detection algorithm finds a peak indicating the existence of a 0° magnet. The z-axis peak detection algorithm finds a peak indicating a 90° magnet. Thus, we can distinguish a lane tag from an information tag. To further decode the information tag, we combine the speed and the heading data from the CAN bus network of the vehicle. By employing Eq. 1, we can precisely calculate the distance ratio of an information tag and thus interpret the embedded lane-specific information.

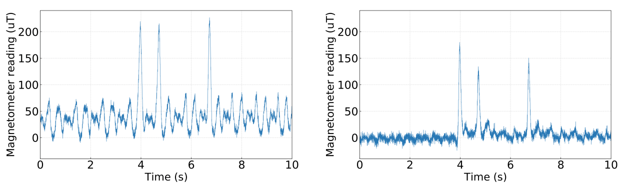

(a) W/ the wheel noise (b) Filtered by AMN

Figure 7: (a) shows the signal with the wheel noise; (b) shows the cancellation performance of AMN.

5.3 Noise Cancellation

For high-accuracy and robust detection, METRO needs to remove real-world noises induced by environmental factors and the ego car. Environmental noises from road infrastructures and bypassing cars can be mitigated by the derivative-based sensing algorithm, as shown in Sec. 7.2.

The key challenge is removing the dynamic noises from the ego car. Specifically, we found the rotation of the car's wheels can incur severe magnetic noises, i.e., frequent spikes in the sensor reading. Fig. 7(a) shows the reading of the sensor in front of the wheel. This dynamic noise may reduce the magnet signals or incur frequent false alerts. Legacy noise cancellation algorithms based on frequency domain analysis, such as wavelet denoising and non-adaptive filters, are not feasible for two reasons. First, the cutoff frequency cannot be determined due to the frequency of the noise varies with the speed. Second, these methods may filter the desired signal of magnets since the frequency components of the noise and the signal are close to each other.

To overcome this problem, we propose a novel denoising scheme called *Adaptive Magnetic field Neutralization* (AMN). It uses two reference sensors mounted in the left and right wheel well. Let s_{front} be the signal of the sensor for detecting magnets in front of the wheel, which contains the periodic noise n_{front} and desired magnet signal s_{mag}, i.e., $s_{front} = n_{front} + s_{mag}$. Each reference sensor records the periodic magnetic noise from the wheel denoted as n_{ref}. Thus, a direct method is to remove n_{front} by utilizing the reference noise n_{ref}. To achieve this, AMN consists of two core steps: sensor coordinate alignment and adaptive noise cancellation.

Step 1, Sensor coordinate alignment. Due to the coordinate system relative to the wheel of these two sensors are different, we choose the coordinate of the front sensor as the reference coordinate, then align the coordinate system of the reference sensor using the rotation transformation.

Step 2, Adaptive noise cancellation. After the coordinate alignment, the reference sensor contains the same feature of wheel noise as the front sensor. However, due to the time delay between these two time-series data, we cannot subtract the aligned sensor reading directly. To solve this problem, we implement an adaptive filter for noise cancellation by using the Least Mean Square (LMS) algorithm. The system structure is shown in Fig. 8. At the initial phase without detecting magnets, AMN first extracts s_{front} and n_{ref} and eliminates the different scale and offset of n_{ref} to s_{front}. Then, we set n_{ref} as the desired signal and s_{front} as the input signal. The filter can extract the signal component from s_{front} that related to n_{ref}

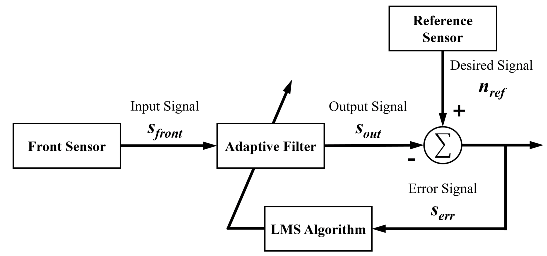

Figure 8: Block diagram of LMS-based filter in AMN.

by yielding the LMS of the error signal s_{err}, i.e., $s_{out} \approx n_{front}$. By subtracting the output signal s_{out} from s_{front}, we can derive s_{mag}.

6 SYSTEM IMPLEMENTATION

6.1 Hardware Configuration

Sensor array construction. We built a sensor array using the standard PCB production process, with a size of 3.2 cm × 177.0 cm. Due to the maximum length limitation of the PCB production (usually 50 cm), for better extensibility and mass production, we divide the long sensor bar into six segments. Each segment is connected with a female and a male pin header efficiently. For reference sensors, the size is 3.2 cm × 3.2 cm. Fig. 9 shows the sensor array and Fig. 10 shows its circuit schematic.

Sensor array configuration. A high sample rate of the magnetometer array is essential for METRO to operate in high-speed scenarios. We choose MLX90393 [10] as our magnetometer chips. Compared to other chipsets, MLX90393 has a wide sensing range (i.e., 5 − 50 mT) and high sample rate of up to 500 Hz. To ensure a high sample rate, we set the sampling ratio (OSR) to 0 and the digital filter (DIG_FILT) to 2. To minimize noise, we tune the gain (GAIN_SEL) and sensor reading resolution (RES) to 7 and 0, respectively.

Data transmission setting. For fast data processing, we choose Teensy 4.1 [13] as our microcontroller unit (MCU), which supports data transmission via USB with a speed of 480 Mbps. We use the SPI [3] protocol over I^2C [2] for fast data communication and synchronization between multiple magnetometers. The aggregated magnetic field measurements are sent to Teensy 4.1 via SPI protocol at a clock frequency of 10 MHz. Then, the data is transmitted to the computing unit (a laptop equipped with an i7-1260P CPU and 16 GB of RAM) via a wired connection with a baud rate of 921,600. Compared to a wireless connection (e.g., Bluetooth), a wired connection enables high-speed data transmission and provides high reliability. Note that the wired transmission can also be incorporated with the CAN bus [68]. The sensor array consists of 14 MLX90393 magnetometers and can achieve an overall sample rate of > **350** Hz. Note that we applied the 350 Hz sampling rate to limit the data synchronization and communication overhead. As we will elaborate in Sec. 7.3, METRO's sensor array can reliably detect on-road magnetic tags even in high-speed scenarios (e.g., > 50 mph) while operating at the sample rate of 350 Hz.

6.2 Magnet Configuration

To find an ideal configuration of passive magnets, we first analyze the magnet flux distribution in the far field of magnets. The

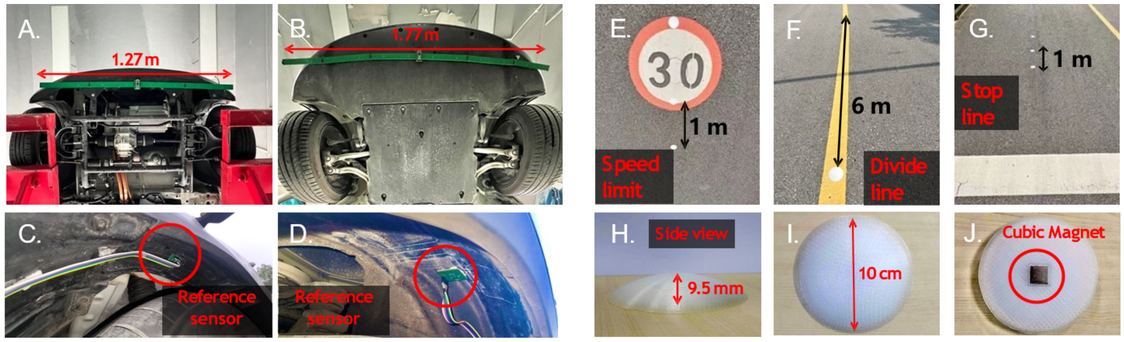

Figure 9: The implementation and deployment of `METRO`. A and B show how the sensor array is installed on commodity cars (a smart electric car and a Tesla Model Y). C and D show the installation of the reference sensor for calibrating the wheel noise. H, I, and J show the `METRO` tag's side, top, and bottom views, respectively. E, F, and G show the exemplary installation of the `METRO` tag on public roads.

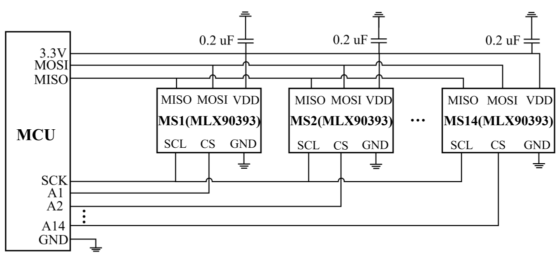

Figure 10: The circuit schematic of `METRO` sensor array.

magnetic field of a spherical magnet with uniform permanent magnetization follows the dipole model [70]. Cylindrical magnets can be modeled by an idealized solenoid [42]. For a cubic magnet, the spherical model is a reasonable approximation for evaluating the field distribution in the far field [35]. Thus, the geometry does not affect the magnetic flux distribution in the far field.

Now, we design the form factor of magnets guided by three key principles, durability, cost-effectiveness, and compact design. Specifically, the magnetic field generated by a magnetic dipole is proportional to its magnetic moment **m**, which is proportional to the residual magnetic flux density **Br** and the volume V of the magnet, i.e., $\mathbf{m} = \frac{1}{\mu_0}\mathbf{Br}V$. Thus, we choose the N52-grade magnet to reduce the size of the magnets due to its high strength-to-size ratio. Moreover, with the same **Br** and V, the magnetic dipole moment is the same. Cuboid magnets can be easily deployed on the road with the N/S polarity for different directions. Thus, cuboid N52-grade neodymium magnets are used for encoding road markings. The length, width, and height of the magnet are 15 mm, 15 mm, and 9.5 mm, respectively.

6.3 System Deployment

Sensor array deployment. For fine-grained sensing, the sensor array is mounted under the front bumper of a vehicle, two reference sensors used for wheel noise cancellation are mounted in the left and right wheel wells separately.

Magnetic tag deployment. For line markings, the most essential principle is to promptly alert the driver when the vehicle begins to move out of its lane. For these markings, magnets are deployed directly above the existing painted markings, i.e., dashed or solid lines. The sensor array can detect the magnet when a vehicle begins to move out of the lane. Then, the vehicle can take action accordingly. To design the inter-magnet distance of two neighboring magnets, we need to balance the trade-off between the lateral deviation distance and detection performance. Specifically, we design the maximal distance to be 6 m. For transverse markings, e.g., straight arrows, the corresponding magnetic tags are deployed on the original road marking in the middle of each lane. For some safety-critical transverse markings, e.g., stop line, the magnetic tags can be deployed a few meters (e.g., 20 m) before to provide sufficient reaction time for drivers.

To improve the resilience of `METRO` against external factors, e.g., being crushed by passing vehicles, we built a PLA-based 3D-printed protective shell. The protective shell is pie-shaped to minimize the impact of vehicles when it is run over. Fig. 9 shows an exemplary deployment. We also examined its practicality (Sec. 8.2) with a one-month deployment on public roads. Our experiment plan was reviewed and approved by our IRB board.

7 EVALUATION

7.1 Experimental Method

Implementation. We use the sensor array aforementioned in Sec. 6.1 and the cuboid magnets as described in Sec. 6.2. We use the magnet with 90° orientation for line markings. For transverse markings, we implement tags consisting of three magnets with 0° orientation; the length and segmentation distances are 4 m and 1 m, respectively. The default tag used in our tests is {"NNN", 0°, 3, 4, 1, 3/1}. We use the x-axis and z-axis time-series data from each magnetometer of the sensor array for detecting 0° and 90° magnets (Sec. 5.2.2). We use the compact electric vehicle (EV) equipped with the `METRO` sensor array in Fig. 9(A) as our testing vehicle, with a ground clearance of 16 cm. A PCAN-USB adapter [7] is used to connect the CAN bus of the testing car. The sample rates of speed and heading angle are 10 Hz and 100 Hz, separately. We synchronize the sample rate to the sensor array (i.e., > 350 Hz) with interpolation.

Figure 11: The emulated traffic jam scenario. A total of 15 vehicles were parked along the roadside.

Evaluation setup. We first evaluate the impact of real-world magnetic field interference, including environmental noises and ego-car noise. Then, we evaluate the impact of different real-world factors (e.g., speed, ground clearance, etc.) for METRO. Finally, we investigate the potential of METRO for a higher encoding capacity with limited length and number of magnets and wider deploying scenarios. We chose a total of three road segments for field tests, including a typical straight road, a rough road, and a 90° curvy road.

Evaluation metrics. For evaluation of the polarity detection performance, we measure the accuracy of detecting N/S polarities. To evaluate the ratio detection performance, we examine the deviation ratio. For example, for a tag with a distance ratio of 3, if the measured distance ratio is 3.012, the corresponding deviation ratio is 3.012/3, i.e., 1.004.

7.2 Real-world Interference

Environmental noises. METRO must differentiate on-road magnetic tags from other environmental noises. Hence, we analyzed the impact of several on-road infrastructures, including manhole covers, speed bumps, and bridge connectors. We mounted the sensor array on the testing car and then drove over each on-road object five times. The experimental results showed that maintenance hole covers, speed bumps and bridge connectors had a negligible effect on the detection pipeline. Specifically, no false positive/negative detection was found from the experimental results.

Disturbances from surrounding vehicles. Now, we analyze the impact of metal structures from surrounding vehicles on the decoding performance of METRO. We employed a public road segment where fifteen vehicles were parked along the roadside to emulate a traffic jam scenario. The total length of this testing road segment was around 80 m. We installed the default information tag (i.e., {"NNN", 0°, 3, 4, 1, 3/1}) in the middle of the testing road. In the experiment, three line tags { "N", 90°} were placed next to the stationary vehicles parked along the roadside with the same longitudinal distance of 6 m, as shown in Fig. 11. Considering the average lane width of 3.6 m and a vehicle width of 1.8 m, the lateral distance between the information tag and the stationary vehicle was set at 2.7 m, and the distance for the line tag was set at 0.9 m. We drove the testing vehicle over these tags with a lateral distance of 0.9 m from the stationary vehicles at 30 mph ten times. The polarity detection accuracy of both tags was 100%, and no erroneous N/S was detected by METRO. This accuracy is enabled by METRO's robust derivative-based peak detection algorithm (Sec. 5.2). The mean and STD of the deviation ratio of the information tag were 0.989 and 0.019, respectively.

	Accuracy	Precision	Recall
W/o AMN	28.8%	37.0%	56.7%
W/ AMN	96.7%	100%	96.7%

Table 1: Noise cancellation performance of AMN.

	Cost	Chip	Size (mm)	Range (m)
Type 1 [26]	$8.4	Alien Higgs 3	$31.7 \times 12.8 \times 4.8$	6
Type 2 [25]	$14.4	NXP UCODE 8	$51 \times 36.3 \times 7.5$	10
Type 3 [24]	$12.8	Monza R6-P	$138.8 \times 42 \times 12$	20

Table 2: The three types of rugged RFID tags.

Ego-car noise. As shown in Sec. 5.3, the periodic noise generated by the rotating front wheels is the major noise for METRO. We verified the AMN algorithm for eliminating the periodic magnetic field noise. We used the sensor directly in front of the left front wheel to detect the magnet. The reference sensor was deployed in the left wheel well, as shown in Fig. 9 (C). We installed three magnets on a straight road, with the inter-magnet distance of 1 meter and 3 meters, respectively, and the polarity orientation is 90°, i.e., N-pole up. We used the z-axis data for the sensing pipeline. We drove the vehicle past these magnets 10 times without using the AMN algorithm at 30 mph. Then, we drove at the same speed with the AMN algorithm. Table 1 shows the polarity detection performance. The AMN algorithm can *greatly* mitigate the periodic noise from wheel rotation in real time. Specifically, using the AMN algorithm, METRO can achieve an accuracy of 96.7%, approximately 70% more than that without AMN.

7.3 Impact of Varying Factors

Watery disturbances. METRO has the advantage over RFID in that water molecules do not attenuate magnetic fields [31]. To demonstrate this, we dug a puddle of 25 cm diameter and 20 cm depth, as shown in Fig. 12(a). Our magnet was placed at the bottom of the puddle, and the depth of the water was varied from 0 to 20cm with 2cm increments. We then took the mean magnetometer readings of 2,000 data points at a height of 25 cm at each depth 10 times. The result, shown in Fig. 12(c), confirms that water does not attenuate the magnetic field. Three types of rugged RFID tags, as shown in Fig. 12(b) and Table 2, are tested. A Chainway C72 handheld RFID reader with an Impinj R2000 chip [15] is employed to measure the received signal strength (RSS) under the same conditions, as shown in Fig. 12(a). The reader operates in a frequency range of 902.75-–927.25 MHz. As shown in Fig. 12(d), the RSS of each tag gets significantly distorted as the depth of the puddle increases.

Vehicle speed. To evaluate METRO's performance at varying vehicle speeds, we ran it on the testing car moving at 15 – 55 mph (i.e., 24 – 88 km/h). 55 mph is the fastest speed we can achieve due to the experiment regulation. Note that adverse weather could reduce vehicle mobility, e.g., speed can be reduced up to 40% under heavy snow, according to FHWA [18] . As shown in Fig. 13(a), the accuracy of detecting 90° and 0° magnets consistently exceeded 93% and 90%, respectively, even at > 50 mph. Then, we evaluated METRO's performance in detecting the information tag 10 times. The

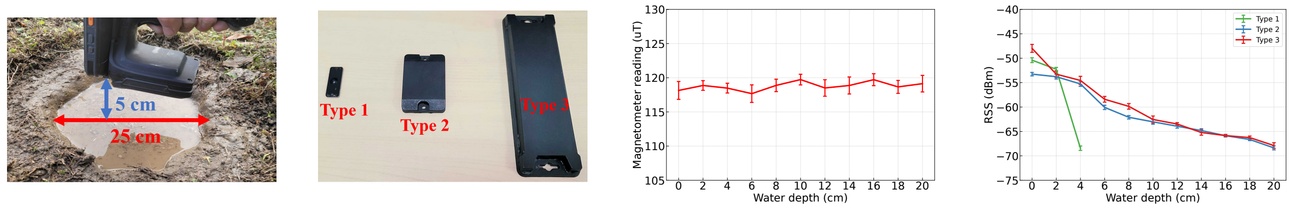

(a) Test scenario (b) Three rugged RFID tags (c) Impact on magnetic field (d) Impact on RSS

Figure 12: Impact of watery disturbances. (a) and (b) show the test settings; (c) and (d) show the result of magnet and RFID tags at varying water depths, respectively.

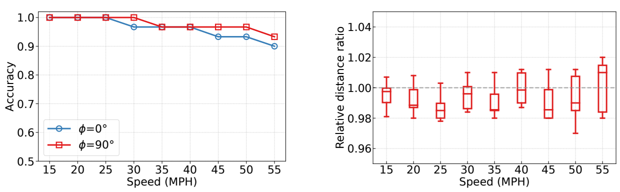

(a) Accuracy w/ different polarities (b) Distance ratio result

Figure 13: The impact of vehicle speed.

distance ratio results are shown in Fig. 13(b), indicating that even at 55 mph, the testing tag was correctly decoded. These results demonstrate METRO's effectiveness in detecting and interpreting METRO tags in high-speed scenarios.

Ground clearance. Due to the limited magnetic field range of a magnet, the sensor height to the ground is essential for the detection performance of METRO. Thus, we focus on the ground clearance, i.e., the shortest distance between a flat ground surface and the undercarriage of vehicle. We first measured the ground clearance of total four typical types of vehicles, including five sedans, five utility vehicles (three SUVs, two pickup trucks), five vans (two minivans, three box vans), and five heavy trucks (two box trucks, three tank trucks), total 20 vehicles. As shown in Fig. 14(a), the average ground clearance are 15.5 cm, 21.1 cm, 28.8 cm, and 37.2 cm separately. According to FHWA's 2021 study [27, 29], light-duty cars, e.g., passenger cars, light trucks, vans, and SUVs, account for about 88.7% of highway traffic.

Thus, we evaluate METRO under a ground clearance ranging from 15 cm to 35 cm. We first evaluate the detection performance of one magnet. We set the orientation to be 90° and 0° for line and transverse markings, respectively. For each polarity orientation, we drove past it 15 times at 30 mph. As shown in Fig. 14(b), both types of magnets can be detected reliably in all tests when the ground clearance is less than 25 cm. Even at 30 cm, the detection performance of line and information magnets are 0.93, and 0.87, respectively. The performance at 35 cm degraded due to the cubic decrease of magnetic field strength with distance. Note that the ground clearance of 30 cm covers the vast majority of real-world vehicle types as shown in Fig. 14(a). For heavy trucks with higher ground clearance, one may tune the sensitivity settings of magnetometers (Sec. 6.1) to improve the detection accuracy. The results also indicate the performance of detecting a 0-degree magnet degrades faster than that of a 90-degree magnet after 25 cm. This observation also justifies the design choice of using 90° for line markings (Sec. 4.1) , as detecting traffic line is more safety-critical.

Then, we evaluated the detection performance of the default information tag, i.e., {"NNN", 0°, 3, 4, 1, 3/1}. Specifically, we tested the detecting performance under 15 cm, 20 cm, 25 cm, 30 cm, and 35 cm, respectively. The experiment of each clearance setting was repeated 10 times. METRO correctly detected the polarities of each tag when the clearance was $\leq$ 30 cm, with an overall accuracy exceeding 97%. At 35 cm, METRO decoded the tag in 5 out of 10 attempts. For all detected cases, the distance ratio result is shown in Fig. 14(c). Therefore, METRO can accurately interpret the magnetic tag within a ground clearance of 30 cm.

Road condition. The road condition (e.g., roughness) may affect the performance of METRO due to the mechanical vibration of the vehicle. To verify this, we use the rough road and test the performance of METRO. We evaluated the impact of using three tag configurations, i.e., tag {"NNN", 0°, 3, 4, 1, 3/1}, tag {"NNN", 0°, 3, 4, 1, 2/2}, and tag {"NNN", 0°, 3, 4, 1, 1/3} . For each tag, we repeat five times at 30 mph. METRO can correctly identify each tag without any miss detection or false alarms in all tests. The distance ratio result is shown in Fig. 15. These three tags can be decoded even under rough road conditions, implying the practicability of METRO.

Temperature. Resilience to harsh temperatures is a critical requirement of road infrastructures. The typical pavement temperature is < 75 °C due to the solar reflectance of paved surfaces [28]. According to the datasheet, the operational temperature of our magnets and sensor array is < 85 °C and -40–85 °C, respectively. We empirically verify their temperature tolerance. We thoroughly heat the magnet for 15 minutes using an HN-25BS temperature chamber [17] from 25 °C to 85 °C with a step of 10 °C while keeping the sensor array at 18 °C. We then took the mean magnetometer reading of 2,000 data points at a height of 25 cm above the magnet for each temperature setting, and repeat it 10 times. For the sensor array (a Teensy 4.1 and an MLX90393 chip), we heat it while keeping the magnet at 18 °C and measure in the same settings. As shown in Fig. 16, the results indicate that high temperatures have a limited impact on the magnet and sensor array. Moreover, we continually heat both the magnet and sensor array at 75 °C for 7 hours. The [mean, STD] of measurement is (89.97, 1.20), further indicating that METRO is highly resilient to harsh temperatures.

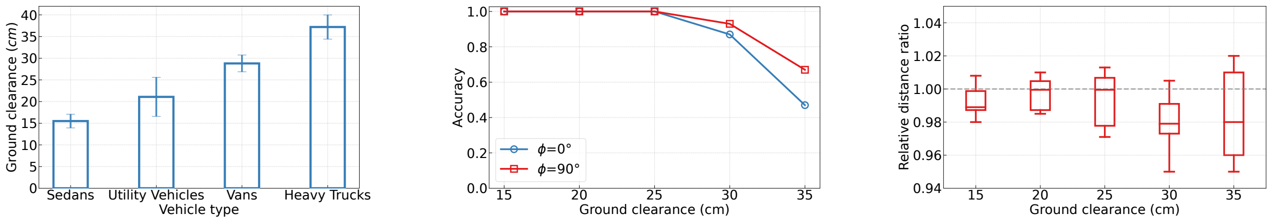

(a) Ground clearances of different cars

(b) Detection acc. w/ different polarities

(c) Distance ratio performance

Figure 14: Impact of vehicle ground clearance.

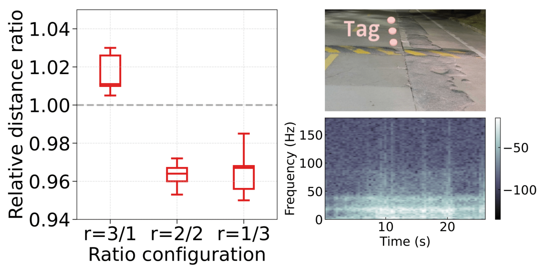

Figure 15: Distance ratio on rough roads.

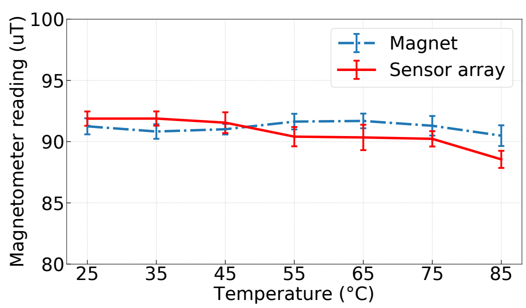

Figure 16: Impact of temperature.

7.4 Encoding Performance of METRO

Varying segmentation distance. The encoding capacity of METRO tags is related to the segmentation distance Seg_d (Sec. 4.2). A small Seg_d enables a large encoding capacity, but it may also lead to erroneous detection of the ratio. To better understand the impact of segmentation distance, we evaluated the detecting and decoding performance with the segmentation distance shrinking from 1 m to 0.02 m. Under each distance setting, we deployed two neighboring tags on the straight road separately and test the detection performance for each tag at 30 mph.

Fig. 17(a) shows the encoding capacity of the 4 m long tag under different segmentation distances according to Eq. (2). Fig. 17(b) shows the detection accuracy of each tag. When $d \geq 0.1$ m, each tag can be detected and decoded correctly. The results indicate that a segmentation distance of *only* 0.1 m is sufficient to decode the METRO tags at high accuracy. This granularity supports encoding *248* types of information with a length of 4 m with only 3 magnets. Note that the results in Fig. 13(b) also demonstrate that even when the segmentation distance was reduced to 0.1 m, METRO can still accurately decode the information tags at 55 mph. This performance suggests a more compact design of METRO tag. One can easily extend

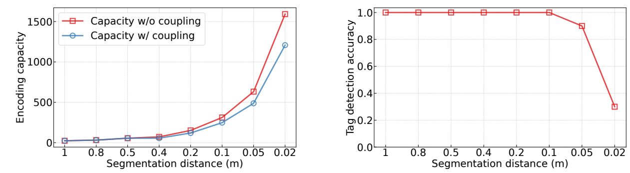

(a) Encoding capacity under different segmentation distances

(b) Detection accuracy with different distances

Figure 17: The impact of segmentation distances.

the encoding capacity by improving the number of magnets and/or tag length (Sec. 4.2).

Curvy road. Compared to the legacy transverse markings, METRO provides the potential of embedding information for the curvy road segments. To evaluate the performance of METRO tags on curvy roads, we placed a tag {"*NNN*", 0°, 3, 6, 1, 3/3} on the curvy road segment and drove pass it at 10 mph 10 times. The experiment results show the [mean, STD] of deviation ratio to be in (0.965, 0.044).

8 PRACTICABILITY ANALYSES OF METRO

To assess METRO's practicability, we analyze its cost, deployability, durability, and usability via field tests on real-world roads and commodity cars.

8.1 Cost Analysis of METRO

METRO sensor array. The hardware cost of a single sensor array, including one Teensy 4.1 ($31.5) and 14 MLX90393 magnetometers ($40) is less than $75. Including the manufacturing cost of PCB production, the total cost would be less than $85 for a regular-sized car (i.e., car width of 1.8 m). Moreover, the sensor array requires minimal maintenance cost thanks to the modular hardware design (Sec. 6.1). For example, replacing a damaged sensor is cost-effective.

METRO tags. The total cost of the N52-grade cuboid magnet we used is $1, including $0.25 for the 3D-printed protective shell. For lane markings, METRO *only* utilizes the polarity of the magnet to digitize different markings, e.g., solid or dashed lines (Sec. 4). Per S-pole or N-pole magnet is installed on the road with an inter-magnet distance of 6m (Sec. 6.3). So, the material cost is $1 per 6m (i.e., $0.17 per meter [65]). In contrast, the traditional marking (paints and thermoplastics) costs $0.21 – 7.70 per meter [4]. For further cost reduction, the magnetic tags for lane markings can be deployed only in accident-prone road segments. For transverse markings (e.g., left arrow), we implemented a tag prototype with three magnets,

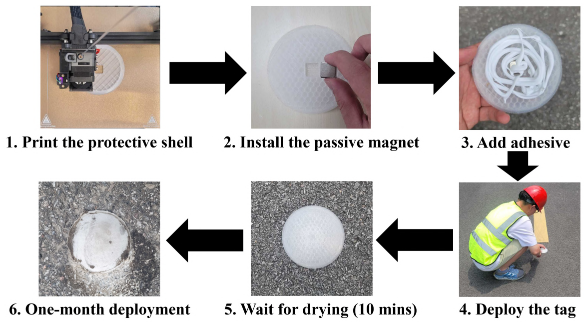

Figure 18: Manufacturing and deploying a METRO tag.

at the cost of $3. In contrast, each rugged RFID tag designed for a similar purpose demands a cost of $8 as described in Sec. 2.

8.2 Deployability of METRO

To evaluate the long-term durability and robustness of METRO in real-world settings, we deployed both the sensor array and tags on a public road for a month.

Long-term deployment. We installed the sensor array under the front bumper of the compact EV used in Sec. 7. To provide further protection against potential damage from road debris, we implemented a PVC shell to shield the sensor array. For the METRO tag, we deployed a line tag { "N", 90°} and an information tag {"SSS", 0°, 3, 2, 1, 1/1} on a busy public road with an average daily traffic volume exceeding 2,200 vehicles based on the statistics from road surveillance over three days, as shown in Fig. 9(F) and (G). The detailed process of manufacturing and deploying a METRO tag is illustrated in Fig. 18. We use epoxy as the adhesive to fix the tag on the road. The deployment process is compatible with the standard installation procedures specified by the FHWA for raised pavement markers [8]. Therefore the installation process would be friendly for construction workers. METRO tags can also be deployed near existing retro-reflectors thanks to their compact design. One can also visually protect the tag by concealing it with asphalt/bitumen coating.

Durability test. During the one-month field testing, the accumulated precipitation was 260 mm, and the highest temperature was 36 °C. The EV equipped with the sensor array covered a total travel distance of over 150 km. The sensor array remained resilient against various factors such as debris, puddles, and vehicle vibrations, i.e., there were no anomalies such as sensor malfunctions or unexpected power loss.

For METRO tags on the road, both the shell and magnet were not damaged as vehicles ran over them. The displacement of each tag caused by running-over vehicles is less than 3mm. This displacement is incurred by the fixation process of the adhesive. After tags were fully fixed to the road in 24 hours, the displacement of each tag was effectively reduced to 0 mm. To assess the impact of road conditions on the magnetic field, such as demagnetization due to adverse weather or distortion caused by accumulated metallic debris, we evaluated the detection performance of METRO. We drove the test EV over the tag at 40 mph for 10 times at the end of the one-month field study. The polarity detection accuracy for both the lane tag and information tag was 100%. Additionally, the [mean, STD] of the deviation ratio of the information tag were (0.993, 0.017), respectively. These empirical studies confirmed the durability and resilience of METRO in real-world road environments. Note that the ultimate deployment scheme should be a collaborative effort of different domain experts (e.g., material science and civil engineering) for further enhancing the lifespan of METRO.

Bumpiness test. We examined if METRO tag would incur uncomfortable bumpiness when the car ran over the tag (with the 3D-printed shell). We quantified the bumpiness by using an embedded accelerometer on the testing car. Specifically, running over the METRO tag only incurs a peak with the amplitude of $< 0.028m/s^2$. This is only 0.0029 G vibration force, thanks to the thin design of METRO tag (Sec. 6).

8.3 Usability of METRO

Now we assess the usability of METRO when road markings are occluded. We evaluate METRO's performance with the most commonly-used road marking detection — the camera-based method [52, 67]. For example, Tesla uses only Tesla Vision [19] for detecting these markings, and has a delivery of more than 1.31 million vehicles in 2022 [22]. In this study, we explore *how* METRO *benefits existing systems.*

We selected three typical road markings: a straight arrow, a left arrow, and a straight-right arrow. To digitize each arrow, we configured the corresponding METRO tag with the following parameters: tag {"NNN", 0°, 3, 2, 1, 1/1}, tag {"SSS", 0°, 3, 2, 1, 1/1}, tag {"SNS", 0°, 3, 2, 1, 1/1}. Then, we *emulated* different levels of snow coverage on the arrows with super-absorbent polymers [48], a common material for artificial snow. We tested three scenarios, i.e., no snow, light snow, and heavy snow, as shown in Fig.19. We implemented a vision-based pipeline based on YOLOv7 [72], a SOTA real-time object detection framework, and trained it with a widely-used road marking dataset, CeyMo, consisting of 2,887 images captured under various adverse conditions [51]. For each emulated snow-covered scenario, we drove the test EV past the arrow straightly at a speed of 15 mph for 10 times. We mounted a OnePlus 9R smartphone on the rear-view mirror to record the video with a resolution of 1920 × 1080 pixels. We processed the video with YOLOv7 on a server with an NVIDIA RTX3080 and 80 GB of RAM.

The results in Table 3 indicate that the performance of the vision-based pipeline is highly affected by the levels of snow, with the pipeline failing to detect any arrow in the heavy snow scenario even at 15 mph. In contrast, METRO operates accurately and reliably even in heavy snow scenarios. Compared to METRO, the vision-based pipeline also requires significantly more computational resources. The side-by-side comparison with the predominant camera-based method suggests that METRO can be a cost-effective complement to existing perception systems. Specifically, METRO would be crucial for extreme environments, e.g., snow squall [14], white-out weather [23], and dust storm [11], as vision-based approaches cannot to "see" road markings.

9 RELATED WORK

In this section, we review related work that aims to improve the road-marking perception with various methodologies.

Figure 19: Testing scenarios. A, D, and G show the no-coverage scenario. B, E, and H represent the light snow condition. C, F, and I emulate the heavy snow setting.

		Straight Arrow			Left Arrow			Straight-Right Arrow		
		No Snow	Light Snow	Heavy Snow	No Snow	Light Snow	Heavy Snow	No Snow	Light Snow	Heavy Snow
METRO	Accuracy	100%	100%	100%	100%	100%	100%	100%	100%	100%
	Distance Ratio	0.99	0.99	1.01	1.00	0.99	1.01	0.99	0.98	0.98
YOLOv7	Accuracy	100%	80%	0	100%	80%	0	100%	70%	0
	Confidence	0.97	0.85	0	0.95	0.81	0	0.91	0.78	0

Table 3: Comparison of METRO and vision-based method.

9.1 Smart Road-to-vehicle Infrastructures

Vision-based schemes. To improve the visibility of road markings, existing road signage systems employ retro-reflective coatings and even LEDs [50, 77]. Augmented reality (AR) enhances road information by overlaying contextual information onto the real-world environment [45]. However, since these approaches rely heavily on computer vision and/or error-prone GPS data for localization, they are ineffective under adverse weather conditions.

Wireless technologies. To address the limitation of vision-based perception, wireless communication is used for smartening road infrastructures. RoS [56] introduces a fully passive and chipless RF tag for digitizing road signs. Millimetro [66] proposes an energy-efficient mmWave retroreflector for accurate long-distance localization. However, these solutions focus on road signs and could only provide coarse-grained information to vehicles/drivers. In contrast, METRO introduces a new road-to-vehicle communication paradigm that enables digitizing lane-specific information and can prevent vehicles from drifting out of the lane.

9.2 Wireless Sensing Techniques

RF-based approaches. RFID has been used to digitize road information, including road signs and lane markers [44, 58]. However, as discussed in Sec. 2 and demonstrated in Sec. 7, it suffers from usability, cost, and durability issues.

Magnetic field sensing. Magnetic fields have been extensively used for enhancing road safety. For example, grid-pattern magnetic markers have been employed to localize the vehicle in places such as intersections [49]. Vehicles can achieve road tracking by strictly following the magnetic path consisting of on-road magnetic markers [16, 34, 36, 47]. However, these systems can not encode rich road information. MagLand [39] matches magnetic fingerprints of existing road infrastructures to detect landmarks. MVP [71] proposes magnetic fingerprint matching to achieve road-level detection. However, such systems require a ground-truth magnetic map before localization/detection. In contrast, METRO can embed rich and detailed lane-specific information into passive magnets by using polarity and distance information (Sec. 4).

10 DISCUSSION

The magnetic field of a passive magnet attenuates with distance cubed. To mitigate the impact of the short sensing range, the tag can be strategically deployed several meters before the visual road paintings. METRO can complement existing solutions (e.g., camera), ensuring the car can detect road markings reliably under adverse weather, thus enhancing overall road safety. Based on our empirical analyses, METRO is suitable for the majority of vehicle types and challenging urban-driving scenarios. The performance degradation is usually caused by driving at high speed (> 50 mph) and high ground clearance (> 30 cm) as shown in Sec. 7.3. Note that cars usually drive slowly in adverse weather. For higher-speed scenarios, e.g., freeways, road markings are sparser and larger in size, so one can improve sensing accuracy by enlarging the tag length. For higher ground clearance, one can use magnetometers with an extended sensing range.

For transverse markings, METRO would be a crucial modality for revolutionizing road marking systems. Specifically, with the enriched encoding capability, METRO can embed detailed road/navigation information in the road marking. For example, for an irregular right turn scenario (e.g., a 125° turn), existing road marking only shows a unified right turn arrow. METRO tag can use magnets to construct detailed direction guidance, e.g., "prepare a 125° right turn". This would help automotive systems to avoid understeer (or oversteer) scenarios, thus protecting driving safety.

11 CONCLUSION

We have presented METRO, the first magnetic road surface marking scheme for monitoring all-weather and smart roads. METRO includes two key design modules: METRO tag and reader. The tag encodes road marking information efficiently with low-cost passive magnets. METRO reader can accurately decode the embedded information. The design of METRO has addressed several challenges in novel ways. For example, it expands the encoding capacity with a limited number of magnets. It also achieves robust sensing performance despite several real-world disturbances. We believe METRO opens doors to a new modality for road marking design, which is essential for the future transportation ecosystem.

ACKNOWLEDGEMENTS

We thank the anonymous reviewers and shepherd for their suggestions. This work was supported by the National Natural Science Foundation of China under Grants No. 6210071207. Dongyao Chen is the corresponding author.

REFERENCES

[1] 1991. Bottsdots. https://www.latimes.com/archives/la-xpm-1991-08-11-mn-779-story.html. (1991).
[2] 2003. I^2C Protocol. https://www.nxp.com/docs/en/application-note/AN10216.pdf. (2003).
[3] 2003. SPI Protocol. https://web.archive.org/web/20150413003534/http://www.ee.nmt.edu/~teare/ee308l/datasheets/S12SPIV3.pdf. (2003).
[4] 2005. Cost-Benefit Analysis. https://www.fhwa.dot.gov/publications/research/safety/humanfac/04142/costest.cfm. (2005).
[5] 2011. The Benefits of Pavement Markings. https://safety.fhwa.dot.gov/roadway_dept/night_visib/pavement_visib/no090488/. (2011).
[6] 2011. Inventor of highway centerline receives international honor. https://www.mlive.com/grand-haven/2011/11/inventor_of_highway_centerline.html. (2011).
[7] 2011. PCAN-USB manual. https://www.peak-system.com/produktcd/Pdf/English/PCAN-USB_UserMan_eng.pdf. (2011).
[8] 2016. Guidelines for the Use of Raised Pavement Markers. https://www.fhwa.dot.gov/publications/research/safety/97152/ch02.cfm. (2016).
[9] 2016. Improved Highway Lane Reflectorized Markers. https://rosap.ntl.bts.gov/view/dot/36357. (2016).
[10] 2017. Melexis: MLX90393 Triaxis® Magnetic Node. https://www.melexis.com/-/media/files/documents/datasheets/mlx90393-datasheet-melexis.pdf. (2017).
[11] 2022. Dust Storm - Wiki. https://en.wikipedia.org/wiki/Dust_storm. (2022).
[12] 2022. How Wide Is The Average Car? (Average Width by Class). https://mechanicbase.com/cars/average-car-width/. (2022).
[13] 2022. Teensy 4.1. https://docs.platformio.org/en/latest/platforms/teensy.html. (2022).
[14] 2022. Watch out for snow squalls, Pa. officials warn. https://www.wesa.fm/environment-energy/2022-11-15/watch-out-for-snow-squalls-pa-officials-warn. (2022).
[15] 2023. Chainway C72 UHF RFID Reader. https://www.chainway.net/Products/Info/42. (2023).
[16] 2023. High-precision, highly reliable autonomous driving achieved by GMPS (Magnetic Positioning System). https://www.aichi-steel.co.jp/ENGLISH/smart/mi/gmps/. (2023).
[17] 2023. HN-25BS Temperature Chamber. https://www.ebay.com/itm/374167813333. (2023).
[18] 2023. How Do Weather Events Impact Roads? https://ops.fhwa.dot.gov/weather/q1_roadimpact.htm. (2023).
[19] 2023a. Replacing Ultrasonic Sensors with Tesla Vision. https://www.tesla.com/support/transitioning-tesla-vision. (2023).
[20] 2023. Repository for METRO. https://github.com/wjk5117/METRO. (2023).
[21] 2023. Rugged RFID Tags. https://www.atlasrfidstore.com/rugged-rfid-tags/. (2023).
[22] 2023b. Tesla Vehicle Production & Deliveries. https://ir.tesla.com/press-release/tesla-vehicle-production-deliveries-and-date-financial-results-webcast-fourth-quarter. (2023).
[23] 2023. Whiteout Weather. https://weather.com/news/weather/news/2023-03-09-weather-words-whiteout. (2023).
[24] 2023a. Xerafy Container Trak RFID Tag. https://www.atlasrfidstore.com/xerafy-container-trak-rfid-tag/. (2023).
[25] 2023b. Xerafy Micro Industrial RFID Tag. https://www.atlasrfidstore.com/xerafy-micro-industrial-rfid-tag-paint-shop-version/. (2023).
[26] 2023c. Xerafy NanoX II RFID Tag. https://www.atlasrfidstore.com/xerafy-nanox-ii-rfid-tag/. (2023).
[27] Federal Highway Administration. 2021a. Highway Statistics 2021. https://www.fhwa.dot.gov/policyinformation/statistics/2021/. (2021).
[28] Federal Highway Administration. 2021b. Pavement Thermal Performance And Contribution To Urban And Global Climate. https://www.fhwa.dot.gov/pavement/sustainability/articles/pavement_thermal.cfm. (2021).
[29] Federal Highway Administration. 2021c. Vehicle miles of travel and related data, by highway category and vehicle type. https://www.fhwa.dot.gov/policyinformation/statistics/2020/vm1.cfm. (2021).
[30] Federal Highway Administration. 2022. Manual on uniform traffic control devices. https://mutcd.fhwa.dot.gov/. (2022).
[31] I.F. Akyildiz, W. Su, Y. Sankarasubramaniam, and E. Cayirci. 2002. Wireless sensor networks: a survey. *Computer Networks* 38, 4 (2002), 393–422. DOI: http://dx.doi.org/https://doi.org/10.1016/S1389-1286(01)00302-4
[32] Salah Azzouzi, Markus Cremer, Uwe Dettmar, Rainer Kronberger, and Thomas Knie. 2011. New measurement results for the localization of UHF RFID transponders using an Angle of Arrival (AoA) approach. In *2011 IEEE International Conference on RFID*. 91–97. DOI: http://dx.doi.org/10.1109/RFID.2011.5764607
[33] Darko Babić, Tomasz E Burghardt, and Dario Babić. 2015. Application and characteristics of waterborne road marking paint. *International Journal for Traffic and Transport Engineering* 5, 2 (2015), 150–169.
[34] Yeun Sub Byun and Young Chol Kim. 2016. Localization Based on Magnetic Markers for an All-Wheel Steering Vehicle. *Sensors* 16, 12 (2016). DOI: http://dx.doi.org/10.3390/s16122015
[35] Juan Manuel Camacho and Victor Sosa. 2013. Alternative method to calculate the magnetic field of permanent magnets with azimuthal symmetry. *Revista mexicana de física E* 59 (06 2013), 8–17.
[36] Ching-Yao Chan and Han-Shue Tan. 2003. Evaluation of magnetic markers as a position reference system for ground vehicle guidance and control. (2003).
[37] Dongyao Chen, Mingke Wang, Chenxi He, Qing Luo, Yasha Iravantchi, Alanson Sample, Kang G. Shin, and Xinbing Wang. 2021a. MagX: Wearable, Untethered Hands Tracking with Passive Magnets. In *Proceedings of the 27th Annual International Conference on Mobile Computing and Networking (MobiCom '21)*. Association for Computing Machinery, New York, NY, USA, 269–282. DOI: http://dx.doi.org/10.1145/3447993.3483260
[38] Zeyuan Chen, Yangchao Wang, Yang Yang, and Dong Liu. 2021b. PSD: Principled Synthetic-to-Real Dehazing Guided by Physical Priors. In *Proceedings of the IEEE/CVF Conference on Computer Vision and Pattern Recognition (CVPR)*. 7180–7189.
[39] Susana B. Cruz and Ana Aguiar. 2020. MagLand: Magnetic Landmarks for Road Vehicle Localization. *IEEE Transactions on Vehicular Technology* 69, 4 (2020), 3654–3667. DOI: http://dx.doi.org/10.1109/TVT.2020.2977599
[40] Chris Debaillon, Paul John Carlson, Yefei He, Thomas Schnell, Fuat Aktan, and others. 2007. *Updates to research on recommended minimum levels for pavement marking retroreflectivity to meet driver night visibility needs.* Technical Report. Turner-Fairbank Highway Research Center.
[41] Farzan Dehbashi, Ali Abedi, Tim Brecht, and Omid Abari. 2021. Verification: Can Wifi Backscatter Replace RFID?. In *Proceedings of the 27th Annual International Conference on Mobile Computing and Networking (MobiCom '21)*. Association for Computing Machinery, New York, NY, USA, 97–107. DOI: http://dx.doi.org/10.1145/3447993.3448622
[42] Norman Derby and Stanislaw Olbert. 2010. Cylindrical magnets and ideal solenoids. *American Journal of Physics* 78, 3 (2010), 229–235. DOI: http://dx.doi.org/10.1119/1.3256157
[43] Paula Fraga-Lamas, Tiago M. Fernández-Caramés, Diego Noceda-Davila, and Miguel Vilar-Montesinos. 2017. RSS stabilization techniques for a real-time passive UHF RFID pipe monitoring system for smart shipyards. In *2017 IEEE International Conference on RFID (RFID)*. 161–166. DOI: http://dx.doi.org/10.1109/RFID.2017.7945603
[44] José Ramón García Oya, Rubén Martín Clemente, Eduardo Hidalgo Fort, Ramón González Carvajal, and Fernando Muñoz Chavero. 2018. Passive RFID-Based Inventory of Traffic Signs on Roads and Urban Environments. *Sensors* 18, 7 (2018). DOI: http://dx.doi.org/10.3390/s18072385
[45] Kevin Gilson, Jagannath Mallela, Paul M Goodrum, and others. 2020. *Leveraging augmented reality for highway construction.* Technical Report. Federal Highway Administration (US).
[46] Sidney Heenan. 1967. Pavement marker. (07 1967). https://patents.google.com/patent/US3332327A/
[47] J.I. Hernandez and Chen-Yuan Kuo. 2003. Steering control of automated vehicles using absolute positioning GPS and magnetic markers. *IEEE Transactions on Vehicular Technology* 52, 1 (2003), 150–161. DOI: http://dx.doi.org/10.1109/TVT.2002.807224
[48] K. Horie, Máximo Barón, R. B. Fox, J. He, M. Hess, J. Kahovec, T. Kitayama, P. Kubisa, E. Maréchal, W. Mormann, R. F. T. Stepto, D. Tabak, J. Vohlídal, E. S. Wilks, and W. J. Work. 2004. Definitions of terms relating to reactions of polymers and to functional polymeric materials (IUPAC Recommendations 2003). *Pure and Applied Chemistry* 76, 4 (2004), 889–906. DOI: http://dx.doi.org/doi:10.1351/pac200476040889
[49] Kyoya Ishii, Keisuke Shimono, Yoshihiro Suda, Takayuki Ando, Tomohiko Nagao, Michiharu Yamamoto, and Masaya Segawa. 2022. Vehicle Localization Using Magnetic Markers Incorporating EKF and Maximum Likelihood Estimation. *IFAC-PapersOnLine* 55, 27 (2022), 202–207. DOI: http://dx.doi.org/https://doi.org/10.1016/j.ifacol.2022.10.512 9th IFAC Symposium on Mechatronic Systems MECHATRONICS 2022.
[50] Shinya Iwasaki, Chinthaka Premachandra, Tomohiro Endo, Toshiaki Fujii, Masayuki Tanimoto, and Yoshikatsu Kimura. 2008. Visible light road-to-vehicle communication using high-speed camera. In *2008 IEEE Intelligent Vehicles Symposium*. 13–18. DOI: http://dx.doi.org/10.1109/IVS.2008.4621155
[51] Oshada Jayasinghe, Sahan Hemachandra, Damith Anhettigama, Shenali Kariyawasam, Ranga Rodrigo, and Peshala Jayasekara. 2022. CeyMo: See More on Roads - A Novel Benchmark Dataset for Road Marking Detection. In *Proceedings of the IEEE/CVF Winter Conference on Applications of Computer Vision (WACV)*. 3104–3113.
[52] Seokju Lee, Junsik Kim, Jae Shin Yoon, Seunghak Shin, Oleksandr Bailo, Namil Kim, Tae-Hee Lee, Hyun Seok Hong, Seung-Hoon Han, and In So Kweon. 2017. VPGNet: Vanishing Point Guided Network for Lane and Road Marking Detection and Recognition. In *2017 IEEE International Conference on Computer Vision (ICCV)*. 1965–1973. DOI: http://dx.doi.org/10.1109/ICCV.2017.215
[53] Yongqing Li, Peng Xiong, Stephan Von Molnár, Steffen Wirth, Yuzo Ohno, and Hideo Ohno. 2002. Hall magnetometry on a single iron nanoparticle. *Applied Physics Letters* 80, 24 (2002), 4644–4646.
[54] Reflecting Roadstuds Ltd. 2022. The Cats Eyes Roadstuds. (2022). https://www.percyshawcatseyes.com/products/the-cats-eyes-roadstuds/

[55] Global News. 2022. 3 killed in massive car collision under heavy snow on Pennsylvania highway - National | Globalnews.ca. (03 2022). https://globalnews.ca/news/8716866/pensylvannia-highway-car-crash-snow/

[56] John Nolan, Kun Qian, and Xinyu Zhang. 2021. RoS: Passive Smart Surface for Roadside-to-Vehicle Communication. In *Proceedings of the 2021 ACM SIGCOMM 2021 Conference (SIGCOMM '21)*. Association for Computing Machinery, New York, NY, USA, 165–178. DOI: http://dx.doi.org/10.1145/3452296.3472896

[57] Neville A. Parker and Massawe S. J. Meja. 2003. Evaluation of Performance of Permanent Pavement Markings. *Transportation Research Record* 1824, 1 (2003), 123–132. DOI: http://dx.doi.org/10.3141/1824-14

[58] Joshué Pérez, Fernando Seco, Vicente Milanés, Antonio Jiménez, Julio C. Díaz, and Teresa De Pedro. 2010. An RFID-Based Intelligent Vehicle Speed Controller Using Active Traffic Signals. *Sensors* 10, 6 (2010), 5872–5887. DOI: http://dx.doi.org/10.3390/s100605872

[59] Fabio Reway, Werner Huber, and Eduardo Parente Ribeiro. 2018. Test Methodology for Vision-Based ADAS Algorithms with an Automotive Camera-in-the-Loop. In *2018 IEEE International Conference on Vehicular Electronics and Safety (ICVES)*. 1–7. DOI: http://dx.doi.org/10.1109/ICVES.2018.8519598

[60] Yoshimichi Sato and Koji Makanae. 2007. Development and Evaluation of In-vehicle Signing System Utilizing RFID tags as Digital Traffic Signs. *International Journal of ITS Research* 4 (01 2007).

[61] Abraham Savitzky and Marcel JE Golay. 1964. Smoothing and differentiation of data by simplified least squares procedures. *Analytical chemistry* 36, 8 (1964), 1627–1639.

[62] Mohsen Shahmohammadi, Matt Chabalko, and Alanson P. Sample. 2016. High-Q, over-coupled tuning for near-field RFID systems. In *2016 IEEE International Conference on RFID (RFID)*. 1–8. DOI: http://dx.doi.org/10.1109/RFID.2016.7488016

[63] Longfei Shangguan and Kyle Jamieson. 2016. The Design and Implementation of a Mobile RFID Tag Sorting Robot. In *Proceedings of the 14th Annual International Conference on Mobile Systems, Applications, and Services (MobiSys '16)*. Association for Computing Machinery, New York, NY, USA, 31–42. DOI: http://dx.doi.org/10.1145/2906388.2906417

[64] Longfei Shangguan, Zhenjiang Li, Zheng Yang, Mo Li, and Yunhao Liu. 2013. OTrack: Order tracking for luggage in mobile RFID systems. In *2013 Proceedings IEEE INFOCOM*. 3066–3074. DOI: http://dx.doi.org/10.1109/INFCOM.2013.6567119

[65] Omar Smadi, Neal Hawkins, Inya Nlenanya, Basak Aldemir-Bektas, and others. 2010. *Pavement markings and safety.* Technical Report. Iowa State University. Institute for Transportation.

[66] Elahe Soltanaghaei, Akarsh Prabhakara, Artur Balanuta, Matthew Anderson, Jan M. Rabaey, Swarun Kumar, and Anthony Rowe. 2021. Millimetro: MmWave Retro-Reflective Tags for Accurate, Long Range Localization. In *Proceedings of the 27th Annual International Conference on Mobile Computing and Networking (MobiCom '21)*. Association for Computing Machinery, New York, NY, USA, 69–82. DOI: http://dx.doi.org/10.1145/3447993.3448627

[67] Ane Dalsnes Storsæter, Kelly Pitera, and Edward McCormack. 2021. Camera-Based Lane Detection—Can Yellow Road Markings Facilitate Automated Driving in Snow? *Vehicles* 3, 4 (2021), 661–690. DOI: http://dx.doi.org/10.3390/vehicles3040040

[68] Craig P Szydlowski. 1992. *CAN specification 2.0: Protocol and implementations.* Technical Report. SAE Technical Paper.

[69] Sunil K. Timalsina, Rabin Bhusal, and Sangman Moh. 2012. NFC and its application to mobile payment: Overview and comparison. In *2012 8th International Conference on Information Science and Digital Content Technology (ICIDT2012)*, Vol. 1. 203–206.

[70] Jean G Van Bladel. 2007. *Electromagnetic fields*. Vol. 19. John Wiley & Sons.

[71] Chia-Cheng Wang, Jyh-Cheng Chen, Yi Chen, Rui-Heng Tu, Jia-Jiun Lee, Yu-Xin Xiao, and Shan-Yu Cai. 2021. MVP: Magnetic Vehicular Positioning System for GNSS-Denied Environments *(MobiCom '21)*. Association for Computing Machinery, New York, NY, USA, 531–544. DOI: http://dx.doi.org/10.1145/3447993.3483264

[72] Chien-Yao Wang, Alexey Bochkovskiy, and Hong-Yuan Mark Liao. 2022. YOLOv7: Trainable bag-of-freebies sets new state-of-the-art for real-time object detectors. *arXiv preprint arXiv:2207.02696* (2022).

[73] Ge Wang, Chen Qian, Longfei Shangguan, Han Ding, Jinsong Han, Kaiyan Cui, Wei Xi, and Jizhong Zhao. 2020. HMO: Ordering RFID Tags with Static Devices in Mobile Environments. *IEEE Transactions on Mobile Computing* 19, 1 (2020), 74–89. DOI: http://dx.doi.org/10.1109/TMC.2018.2890520

[74] Ju Wang, Liqiong Chang, Omid Abari, and Srinivasan Keshav. 2019. Are RFID Sensing Systems Ready for the Real World?. In *Proceedings of the 17th Annual International Conference on Mobile Systems, Applications, and Services (MobiSys '19)*. Association for Computing Machinery, New York, NY, USA, 366–377. DOI: http://dx.doi.org/10.1145/3307334.3326084

[75] Jue Wang and Dina Katabi. 2013. Dude, Where's My Card? RFID Positioning That Works with Multipath and Non-Line of Sight. *SIGCOMM Comput. Commun. Rev.* 43, 4 (aug 2013), 51–62. DOI: http://dx.doi.org/10.1145/2534169.2486029

[76] Mingke Wang, Qing Luo, Yasha Iravantchi, Xiaomeng Chen, Alanson Sample, Kang G. Shin, Xiaohua Tian, Xinbing Wang, and Dongyao Chen. 2022. Automatic Calibration of Magnetic Tracking. In *Proceedings of the 28th Annual International Conference on Mobile Computing And Networking (MobiCom '22)*. Association for Computing Machinery, New York, NY, USA, 391–404. DOI: http://dx.doi.org/10.1145/3495243.3558760

[77] Purui Wang, Lilei Feng, Guojun Chen, Chenren Xu, Yue Wu, Kenuo Xu, Guobin Shen, Kuntai Du, Gang Huang, and Xuanzhe Liu. 2020a. Renovating Road Signs for Infrastructure-to-Vehicle Networking: A Visible Light Backscatter Communication and Networking Approach. In *Proceedings of the 26th Annual International Conference on Mobile Computing and Networking (MobiCom '20)*. Association for Computing Machinery, New York, NY, USA, Article 6, 13 pages. DOI: http://dx.doi.org/10.1145/3372224.3380883

[78] Song Wang, Jingqi Huang, and Xinyu Zhang. 2020b. Demystifying Millimeter-Wave V2X: Towards Robust and Efficient Directional Connectivity under High Mobility. In *Proceedings of the 26th Annual International Conference on Mobile Computing and Networking (MobiCom '20)*. Association for Computing Machinery, New York, NY, USA, Article 51, 14 pages. DOI: http://dx.doi.org/10.1145/3372224.3419208

[79] Lei Yang, Yekui Chen, Xiang-Yang Li, Chaowei Xiao, Mo Li, and Yunhao Liu. 2014. Tagoram: Real-Time Tracking of Mobile RFID Tags to High Precision Using COTS Devices. In *Proceedings of the 20th Annual International Conference on Mobile Computing and Networking (MobiCom '14)*. Association for Computing Machinery, New York, NY, USA, 237–248. DOI: http://dx.doi.org/10.1145/2639108.2639111

[80] Renjie Zhao, Purui Wang, Yunfei Ma, Pengyu Zhang, Hongqiang Harry Liu, Xianshang Lin, Xinyu Zhang, Chenren Xu, and Ming Zhang. 2020. NFC+: Breaking NFC Networking Limits through Resonance Engineering. In *Proceedings of the Annual Conference of the ACM Special Interest Group on Data Communication on the Applications, Technologies, Architectures, and Protocols for Computer Communication (SIGCOMM '20)*. Association for Computing Machinery, New York, NY, USA, 694–707. DOI: http://dx.doi.org/10.1145/3387514.3406219

[81] Tu Zheng, Yifei Huang, Yang Liu, Wenjian Tang, Zheng Yang, Deng Cai, and Xiaofei He. 2022. CLRNet: Cross Layer Refinement Network for Lane Detection. In *Proceedings of the IEEE/CVF Conference on Computer Vision and Pattern Recognition (CVPR)*. 898–907.

[82] Helmut T Zwahlen and Thomas Schnell. 1995. Visibility of new pavement markings at night under low-beam illumination. *Transportation Research Record* 1495 (1995), 117.